Magnetic structure and microstructure of die-upset hard magnets $RE_{13.75}Fe_{80.25}B_6$ (RE=Nd, Pr): A possible origin of high coercivity

V. V. Volkov[a] and Y. Zhu
Department of Applied Science, Brookhaven National Laboratory, Upton, New York 11973

(Received 27 August 1998; accepted for publication 21 December 1998)

In situ transmission electron microscopy magnetizing experiments combined with Lorentz magnetic microscopy in Fresnel–Foucault modes were used to characterize the magnetic structure of die-upset, high energy-product hard magnets $Nd_{13.75}Fe_{80.25}B_6$ and $Pr_{13.75}Fe_{80.25}B_6$. Experimental observations indicate a well-aligned grain structure and quasiperiodic nonaligned ''extended defect'' layers transverse to press direction. The local remanence of the ''defect'' layers is far from saturation when the external field is removed. The layers are enriched with inclusions of approximate composition Nd_7Fe_3, generally with a polygonal shape, and are associated with the original ribbon interfaces. They may be responsible for a high coercivity mechanism, since the motion of reverse domains can be impeded by these layers, even when they are nucleated. Thus, a delayed nucleation of reversed domains seems to be a limiting factor for magnetization reversal and coercivity force. Both Lorentz magnetic imaging and high-resolution microscopy highlight the role of magnetocrystalline anisotropy for domain wall-grain boundary interactions and pinning. Local remanence was estimated directly from magnetic moment sensitive Foucault images. © *1999 American Institute of Physics.* [S0021-8979(99)07106-6]

I. INTRODUCTION

The magnetic properties of permanent magnets are sensitive to their microstructure. In particular, for a family of Nd(Pr)–Fe–B magnets a very different coercivity and energy products may be obtained by several processing techniques. It was experimentally found that a small excess of Nd over the exact phase composition of $Nd_2Fe_{14}B$ plays an important role in obtaining high-energy products during the die-upset processing of the anisotropic hard magnets.[1–3] However, the specific role of the Nd excess on both magnetic structure and microstructure of these die-upset magnets is unclear and controversial. There are some experimental observations using transmission electron microscopy (TEM) on good quality hot-pressed and die-upset magnets Nd–Fe–B,[1,2,4] where the presence of small inclusions of secondary phases with approximate composition Nd_3Fe was reported, but their relation to high coercivity was not analyzed in detail. On the other hand, several articles[4,5] reported on the improvement of intrinsic coercivity of the hard magnets by introducing nonmagnetic phases or dispersoids.

The question of grain alignment and its relation to magnetic domain (MD) configurations in highly anisotropic die-upset Nd–Fe–B magnets also received some attention. Answers to these questions may help to correctly address some major issues in materials science, e.g., how microstructure is related to magnetic structure of hard magnets, and how to optimize the performance of hard magnet. The aim of the present article is *in situ* examinations of MD configurations, and domain wall (DW) motion in die-upset Nd(Pr)–Fe–B magnets under different applied fields, and structural analyses of their possible relation to grain alignment, magnetic parameters, and composition. We discuss the phenomenon of high coercivity in die-upset Nd–Fe–B hard magnets, and give some new insights on its origin in terms of nonaligned ''defect layers'' on the basis of our experimental data. The results were obtained by the use of Lorentz microscopy both in Fresnel and Foucault mode for imaging MD configurations, along with analyses of electron diffraction, energy-dispersive x-ray spectroscopy (EDS), and high resolution electron microscopy (HREM). We emphasize the Foucault imaging technique since it allows us to simultaneously reveal the configurations of both MD and crystalline grains. We introduce the concept of the *reverse domain tip* (RDT), which was found to be very fruitful for explaining *in situ* magnetizing experiments. Some new experimentally observed fine details of the interaction between MD and grain boundaries (GBs) will be discussed as well.

II. MICROSTRUCTURE MODELS OF COERCIVITY

To our knowledge, there is no well-acceptable microstructural model for the origin of coercivity in die-upset magnets. The phenomenological models available operate with some ''effective best-fit'' parameters, which do not give clear insight into the magnetic structure nor the details of the microstructure. Therefore, any new microstructural model would be valuable. Ideally, it should explain at least some experimentally observed correlations. In practice, an increase in remanence I_r (Wb/m^2) or $4\pi M_r$ (kG), where M_r is magnetization, is accompanied by a decrease in the coercive field $H_{ci,}$ and vice versa. Mathematically, this can be expressed, for instance, by a linear equation such as $M_r+\beta H_c\approx$ Const, where $M_r=mM_s$, and M_s is saturated moment. We assume, of course, that any additives or secondary phases do not greatly change M_r since its value is governed primarily by

[a]Electronic mail: volkov@bnl.gov

 © 1999 American Institute of Physics

the microstructure of the matrix. A few fruitful models, based on this point of view, and satisfying the above conditions were proposed.

Hirosawa *et al.*[6] showed that the nucleation field, made up of the sum of the intrinsic coercivity and the effective demagnetizing field, I_s ($\equiv 4\pi M_s$), is linearly related to the effective anisotropy field of the $RE_2Fe_{14}B$ phase. Thus, $(iH_c+I_s)=cH_a$, where cH_a is the effective field necessary for domain reversal (for $Nd_2Fe_{14}B$, anisotropy field $H_a=73$ kOe,[7] and ''c'' is a slope of the linear fit, which was found to be 0.38 by Hirosawa *et al.*[6] and 4.26 by Ramesh *et al.*[4] for Ho-substituted sintered Nd–Fe–B magnets.

Building on earlier work of Durst and Kronmuller,[8] a similar but slightly modified formula $\mu_o H_c(T) = \alpha_{ex}\alpha_k\mu_o H_N^{min}(T) - N_{eff}I_s(T)$ for nanocrystalline NdFeB magnets was discussed by Zern *et al.*[9] in relation to Brown's paradox, which states that the coercive field H_c of a real magnet microstructure is much lower than the theoretically predicted one. Here, the so-called microstructural (best-fit) parameters α_k, α_{ex}, and N_{eff} were assumed to account for the nonideal microstructure of the real magnet. Originally, the effective anisotropy field H_N[8] was assumed to be equal to $2K_1/I_s(=73$ kOe); however, recently[9] it was reduced to $H_N^{min}=K_1/I_s$.[10]

A rough estimate of coercive field H_{ci} for the nucleation mechanism was made by Livingston,[11] who suggested that $H_{ci}=\gamma_w/(r_o M_s) - N_{eff}(4\pi M_s)$, where the first term means the local internal field necessary to nucleate a reverse domain in a spherical defect of radius r_o, and the second term is an effective demagnetization field that assists reversal. Here, γ_w and M_s mean the DW energy and saturated magnetization, respectively. A similar, but slightly modified formula for the analysis of mechanically alloyed and melt-spun NdDyFeB magnets was used by Villas–Boas *et al.*[12] in the framework of the so-called global model of coercivity, based on magnetic viscosity measurements.[13]

It is difficult experimentally to differentiate between the various proposed mechanisms for domain reversal and nucleation. Therefore, in the present article, we report some new experimental TEM data, which can justify some of the above formulas for H_c from the microstructural point of view; and may be useful for further development of an accurate microstructural model of high coercivity in die-upset magnets.

III. EXPERIMENT

The magnet samples used in this study, with nominal compositions $Nd_{13.75}Fe_{80.25}B_6$ [hot-pressed HP1553 (MQ-2) and die-upset DU1418 (MQ-3)] and $Pr_{13.75}Fe_{80.25}B_6$ (die-upset DU1929), were produced at the General Motors Research and Development Center. All samples had high energy products. For instance, sample DU1418, mostly studied in this work, had the energy product $(BH)_{max}=36.38$ MGOe, remanence $B_r=12.9$ kG, and intrinsic coercivity $H_{ci}=18.9$ kOe.[14] Buttons of samples were prepared from overquenched ribbons using the melt-spun technique followed by a hot-pressing procedure,[15] i.e., the melt-spun ribbon was crushed into polycrystalline flakes that are hot pressed (to $P=100$ kPa or 15 kpsi) in vacuum or inert atmosphere at about 700 °C into a fully dense ($D_m=7.55$ g/cm^3), fully crystalline isotropic magnet. This material is known as MQ-2 (MQ stands for the trade mark name MagneQuench). The pressing parameters for MQ-2 are not critical above 700–750 °C when a sufficient plasticity of the material is reached.[15] If MQ-2 is further compressed in a closed die at about 750–800 °C with initial strain rate about 2×10^{-2}, it develops a strong crystallographic texture with the c-axis parallel to the compression direction. Usually the applied pressure of ~10 kpsi for a few seconds at 750 °C is sufficient for 50% plastic deformation (i.e., 50% thermomechanically deformed or die-upset magnet).[16] This material is known as MQ-3, which is magnetically anisotropic.

A few TEM specimens for each sample were prepared for structural characterization. Thin sections were first cut from the buttons, mechanically polished, and then ion milled until perforation. Both magnetic imaging and electron microscopy studies were performed on a standard JEM 2000FX microscope operating at 200 kV. The local composition of some grains and several inclusions were analyzed using a LINK EDS system attached to microscope. The specimen was tilted to vary the in-plane field direction to study the *in situ* MD configurations generated and their interaction with microstructural defects. The specimens were magnetized with the magnetic field of the objective lens ($\mu_o H\approx 1.9$ T).

IV. RESULTS

A. Domain structure and local magnetization imaging

Before analyzing the experimental results, it is useful to recall some specific features of the phase sensitive Foucault images used for magnetic domain analysis of uniaxial magnetic structures. For a relatively big crystalline grain that exceeds single-domain grain size D_c, multidomain configurations are observed. Such a grain may consist of several ferromagnetic domains separated by 180° Bloch walls of specific thickness (δ_o) with the antiparallel alignment of single domain moments (m_s). Figure 1(a) is an experimental Foucault image of such a multidomain structure for demagnetized $Nd_2Fe_{14}B$ grains viewed approximately perpendicular to the c axis (the quality of such magnetic images is very sensitive to the position of the selected-area aperture used). Here, the ratio of domain thickness with magnetic spins up (D_u, black domains) to that of with magnetic spins down (D_d, white domains) is close to unity. For partially magnetized or nonuniformly magnetized samples, the local MD configurations may look like those schematically shown in Figs. 1(b) and 1(c). The local magnetization of sample can then be easily estimated in the following way. First, a ratio of fractional surface areas S_u/S_d covered with white and black domains within the so-called ''magnetic probe cell'' should be estimated. Such a probe cell [shown as a frame in Fig. 1(b)] must contain at least 2 or more even domains of different color to satisfy the translation property. Then, the normalized local magnetization (I_r) can be directly determined from the Foucault image by a simple relationship:

$$I_r/I_s = m = (1 - S_d/S_u) \approx (1 - D_d/D_u), \quad (1)$$

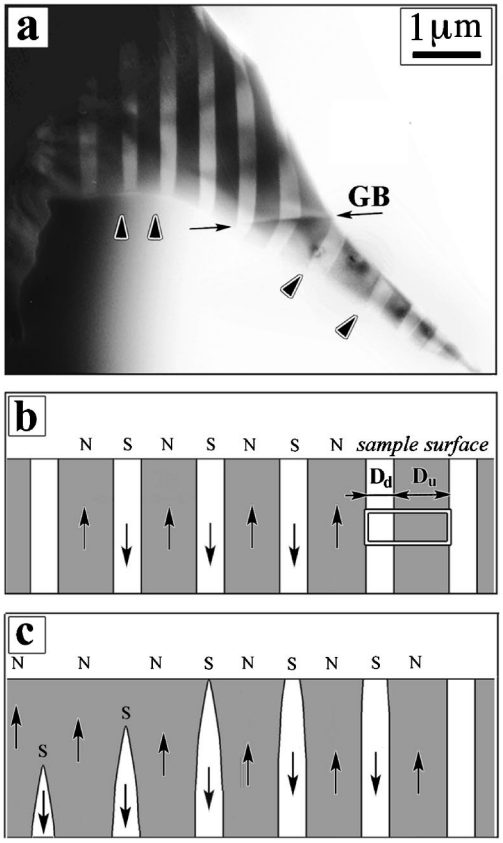

FIG. 1. Foucault image (a) of multidomain magnetic structure of $Nd_2Fe_{14}B$ grains, viewed with major in-plane c-axis components. Note the continuity of the domain walls across the GB with the walls parallel along the local easy magnetic direction (c axis) of the grains. Schematic drawings of a partially magnetized (b), and nonuniformly magnetized (c) magnetic domain structure.

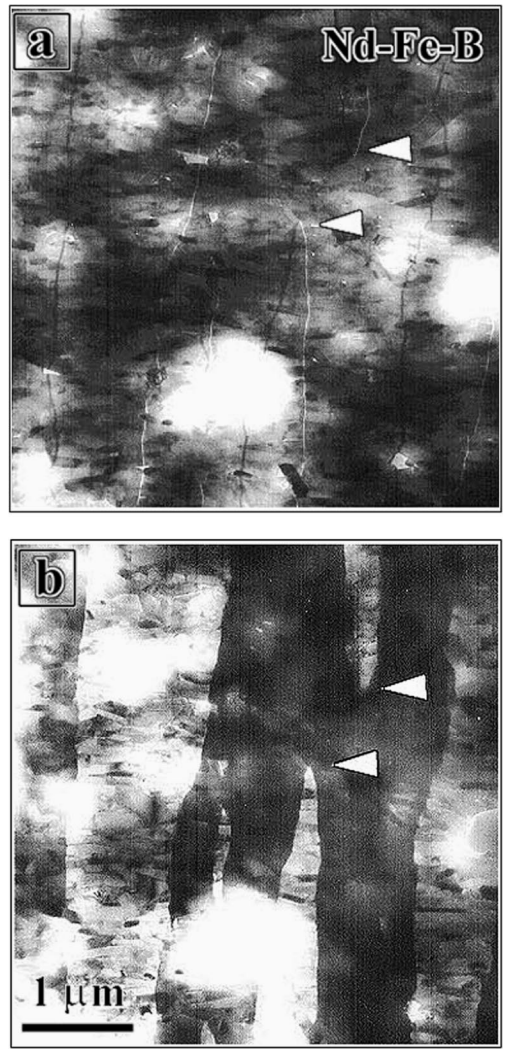

FIG. 2. Fresnel (a) and Foucault (b) images of the same well-aligned grain area of die-upset magnet $Nd_{13.75}Fe_{80.25}B_6$ (DU1418, MQ-3) in an almost demagnetized state, as evaluated from formula (1). Note the small flack-like contrast lines perpendicular to DWs are the crystalline grains with an average size 250×25 nm^2. Large arrows in (b) mark the reverse domain tips.

where I_s is saturated magnetization ($I_s \approx 1.6$ T for $Nd_2Fe_{14}B$[7]), $S_u = \mathbf{e}\mathbf{D}_u$ and $S_d = \mathbf{e}\mathbf{D}_d$ are the surface areas of antiparallel aligned domains which, in turn, are proportional to their widths D_u and D_d ($D_d \neq 0$). Here $S_u > S_d$ was assumed and $\mathbf{e}$ is a unit vector along the direction of saturated moment M_s. For instance, the local remanence in Fig. 1(b) differs from zero since D_u/D_d or $S_u/S_d \neq 1$. Thus, the Foucault images can be readily used for qualitative/quantitative analysis of MD configurations, discussed below.

B. Microstructure and grain alignment

One of the unique capabilities of the Foucault imaging mode is that both the magnetic and grain structural features can be observed in one image. Usually, the domain structure in Foucault images is visible as alternative sequence of lamellae of black and white contrast [Fig. 1(a)], which differ from the gray contrast of grain interfaces.

The microstructure of hot-deformed magnets is highly anisotropic, as shown in cross-section view [Figs. 2(a), 2(b), 3(b), and 3(c)] and in plane-view [Fig. 3(a)]. The materials mainly consist of small platelet-shaped grains of the $Nd(Pr)_2Fe_{14}B$ phase, separated by a thin intergranular phase less than 2 nm thick. Most small grains are stacked together, such that their flat facets (a-b planes) are aligned predominantly perpendicular to the die-upset direction (Figs. 2, 3(b), and 3(c): area B), which is parallel to the averaged c-axis direction. Such c-axis aligned platelet grains and their associated MD structure directly contribute to the high remanence of die-upset samples.

Nonaligned grains of over 300 nm in size were also found in the die-upset samples. However, they occur predominantly within certain areas, which we call ''defect layers,'' since the major areas of well-aligned grains are almost free of them. Our observations indicate that the fine structure of such defect layers varies. For instance, in the die-upset sample (DU1418), such nonaligned grains were separated or mixed with non magnetic inclusions (Fig. 4) that are Nd rich with approximate composition Nd_7Fe_3, as deduced from local EDS-composition analysis, and consistent with the observations of Mishra.[2] Nonaligned larger grains over 400 nm with multidomain structure ($D > D_c$) were found in sample DU1929 [Fig. 3(b), area A]. In contrast to small aligned grains of 2-14-1 phase, the multidomain-containing large grains in DU1929 usually do not have preferential orienta-

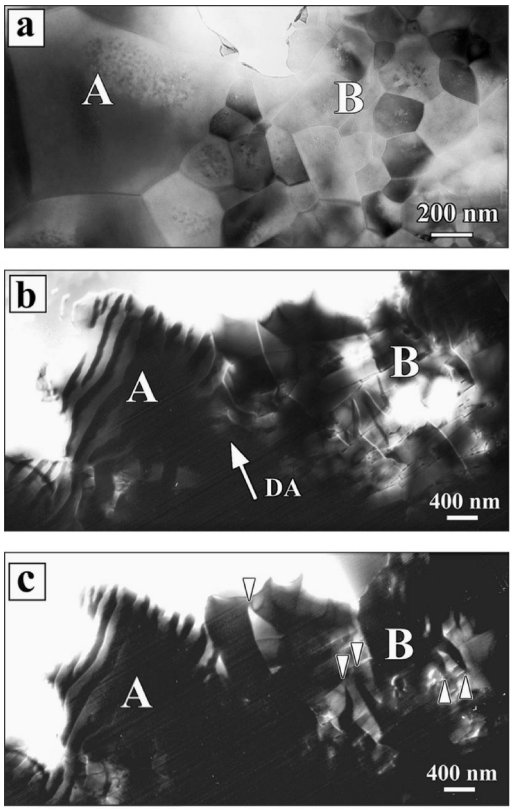

FIG. 3. Not well aligned grains of a $Pr_{13.75}Fe_{80.25}B_6$ (DU1929) hard magnet viewed approximately along the c axis in normal TEM mode (a), and perpendicular to the c axis (b),(c) in a mixed Frensel–Foucault mode as complementary images. Small dot contrast within the grains in (a) is the Nd-enriched phase precipitates. Notice that the domain tips are easily pinned by grain boundaries. Big grains ($D>D_c$) have a well developed multidomain structure with random easy magnetic axis orientation with respect to the die-upset (DA) direction, marked with a big arrow in (b).

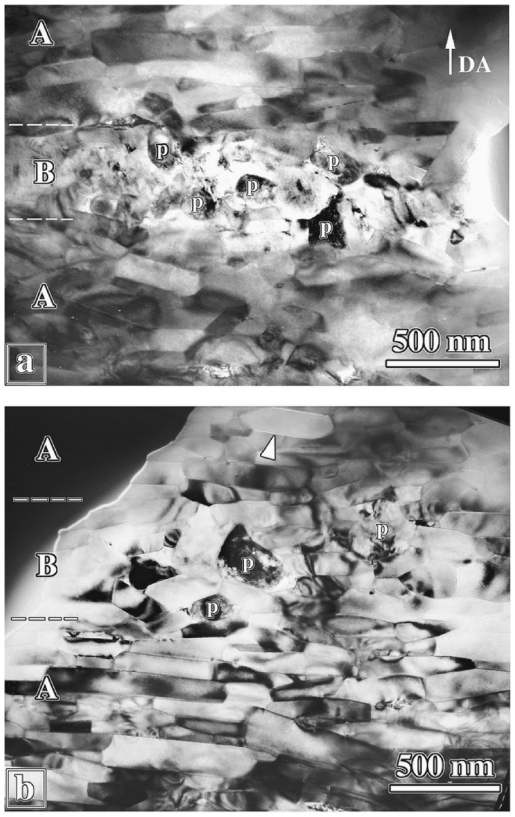

FIG. 4. Two typical bright-field images (a),(b) of the defect layers (marked as B) sandwiched between two well-aligned layers (marked as A) in the microstructure of die-upset hard magnet $Nd_{13.75}Fe_{80.25}B_6$ (DU1418). The presence of nonmagnetic Nd-rich inclusions (marked as p) of polygonal shape within the defect layer may contribute the poor alignment of platelet-shaped grains of the magnetic phase.

tions. The MDs, separated by 180° Bloch walls, are usually parallel to the local grain crystallographic c axis (easy magnetic axis), which, in turn, does not correlate straightforwardly to the hot-pressed direction [Fig. 3(b): area A]. We note that the major parts of well-aligned grain areas are almost free of defect layers. Hence, a microstructure may be considered as consisting of relatively thick layers (A) of well-aligned grains separated by thin defect layers (B) of nonaligned grains (Fig. 4: area A and B). The thickness of these layers was estimated as 4–6 and 0.5–1.0 μm, respectively, with a total period of ''quasisuperlattice'' about 5–7 μm. The magnetic domain structure is also quasiperiodically interrupted by these defect layers, as deduced from the Foucault image in Fig. 5, showing the MD configurations in the vicinity of defect layer. We believe that such quasiperiodical defect-layered microstructure originates from the not-vanished interfaces between the ribbons and flakes used to form the dense die-upset hard magnets.[15,16] For cross-section samples, the occurrence of ribbon boundaries with a period about 5–7 μm can be easily delineated in the optical microscope by a selective etchant. These observations agree well with those mentioned in Refs. 2, 15, and 16.

Because only well-aligned plate-shape grains and their MD structure strongly correlate with die-upset direction, they directly contribute to high remanence of anisotropic die-upset samples. The nonaligned grains with random orientations contribute much less to remanence (such as area B in Fig. 5). The remanence I_r/I_s of the hot pressed sample (isotropic magnet MQ-2, sample HP1553) was found experimentally to be 0.60(4). After the die-upset procedure its remanence increased to 0.83(4) (anisotropic magnet MQ-3, sample DU1418[14]). Both values of remanence obtained can be explained in terms of much better grain alignment after the die-upset procedure. For $I_r/I_s = 0.60(4)$, we estimated that the maximum angle θ_o, deviating from the c-axis alignment, was 75°-85°, i.e., close to the ideal $\theta_{max}=90°$-angle distribution for random orientation of grains [for details, see Sec. V A, formula (3)]. Such small deviations from θ_{max} may occur due to presence of weak magnetic texture in the hot pressed magnet[15,16] or weak remanence enhancement caused by exchange coupling near the grain interfaces. The absence of preferential grain alignment in HP-1553 was also confirmed by TEM observations. Because of specific defect-layered microstructure, quantitative description of the die-upset sample DU1418, will be also given in Secs. V A and V C.

C. *In situ* TEM magnetizing experiments

As shown in Figs. 2–6, the major structural feature of the die-upset samples $RE_{13.75}Fe_{80.25}B_6$ (RE=Nd, Pr) is the alternation of well aligned and not well aligned crystalline

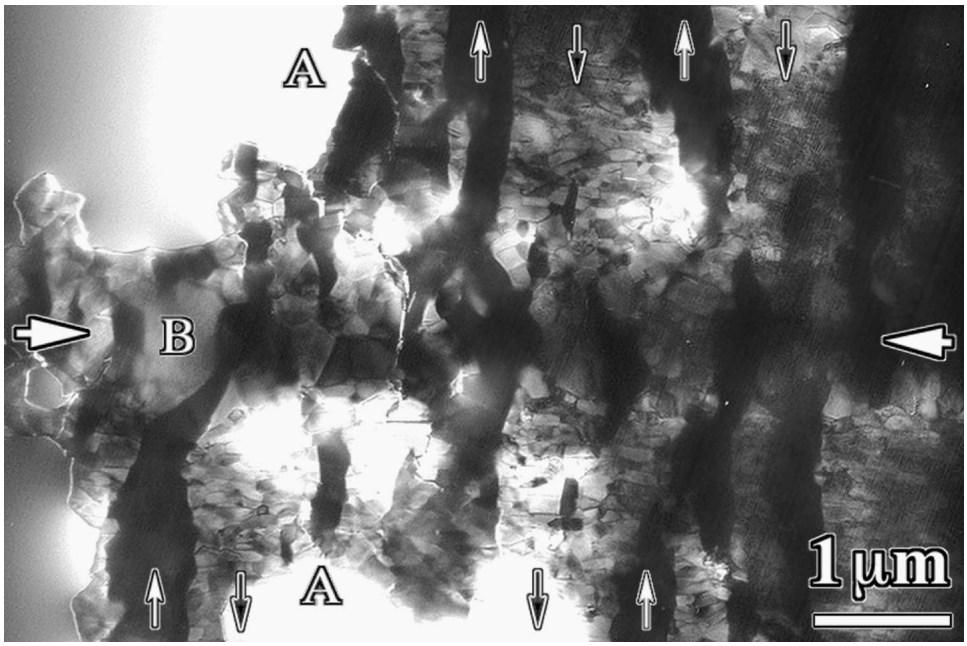

FIG. 5. Foucault image of the observed magnetic domain structure in the vicinity of defect layer (area B indicated by the pair of arrows) in die-upset magnet $Nd_{13.75}Fe_{80.25}B_6$ (DU1418). Note the interruption, reversal and splitting of the MDs when they approach defect layer from the ''perfect'' well-aligned grain layers.

grains. By applying external field, our magnetic TEM experiments indicate that big grains with a multidomain structure ($D > D_c$) may relatively easily be magnetized or demagnetized. Small grains ($D \leqslant D_c$), on the other hand, have either domain walls wrapped around individual grains or several well-aligned grains bounded by ferromagnetic exchange interactions ($D < D_c$) into a single MD (Fig. 2). Reverse domain tips (RDT) may interact with grain boundaries, as marked by arrowheads in area B of Fig. 3(c). We note that the domain tips were often pinned by nonaligned grain interfaces, but do not interact with well-aligned grain boundaries. We found MD-pinning conditions at the grain interfaces are sensitive to the grain misorientation, composition, and the thickness of the intergranular phase (also see Sec. IV D). Therefore, different grain boundaries, along with local grain misalignment may have different abilities to act as effective

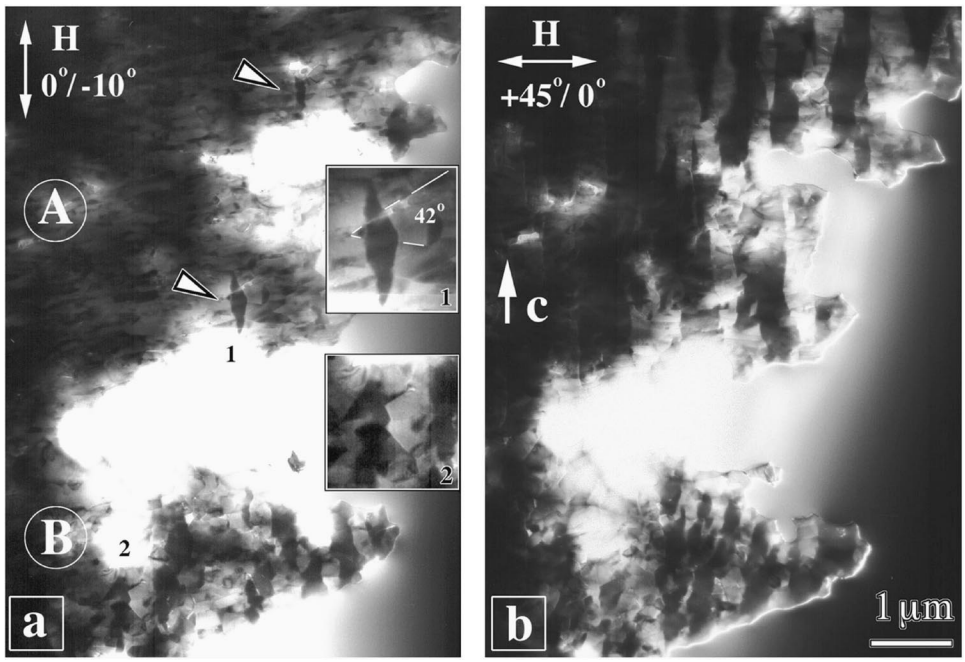

FIG. 6. Foucault images of remanence magnetization of a die-upset magnet $Nd_{13.75}Fe_{80.25}B_6$ (DU1418) after saturation with the in-plane component of an external magnetic field applied along the easy magnetic axis (a) and the heavy magnetic axis (b) by properly tilting the specimen. Note that the area A, composed of well-aligned grains, remains magnetically saturated in (a), whereas area B (defect layer) is far from saturation. Insets in (a) show the presence of small reverse domains.

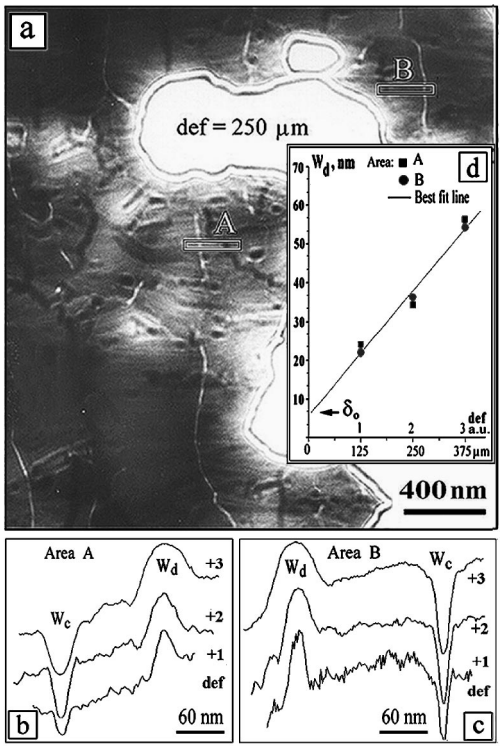

FIG. 7. Fresnel image (a) of domain structure for die-upset magnet (sample DU1418, MQ-3). Line profiles in (b),(c) correspond to A and B selected areas in (a). The DW width is determined as zero-asymptotic of FWHM intensity peaks across DW images vs the defocus value (b,c).

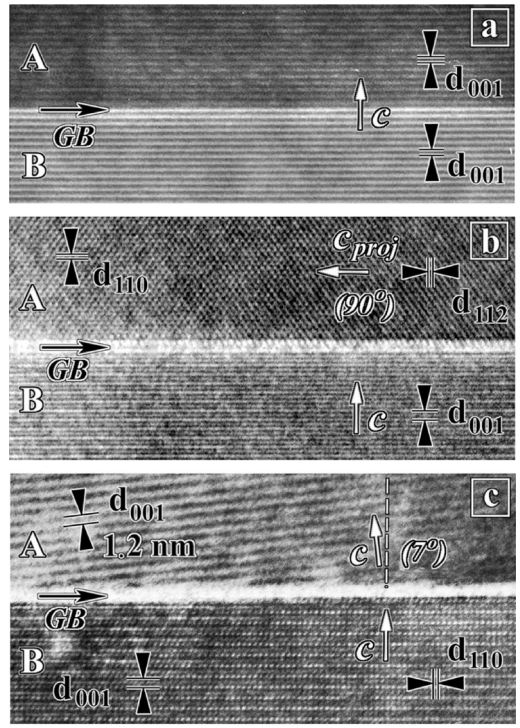

FIG. 8. HREM images of large-angle grain boundaries in magnet $Pr_{13.75}Fe_{80.25}B_6$ (DU1929) (a),(c) and $Nd_{13.75}Fe_{80.25}B_6$ (DU1418) (b). A crystalline and an amorphized intergranular phase is visible in (b) and (c), respectively, but not in (a). The boundary planes are: (a) $(001)_A//(001)_B$, (b) $(110)_A//(001)_B$, and (c) $(109)_A//(001)_B$. GB indicates the position of a grain boundary, while $d_{112}, d_{110}, d_{001}, d_{002}$ show the spacing of the corresponding lattice planes. White arrows show the direction of c axes (easy magnetic directions) in A and B crystals.

pinning centers. Such possible strong pinning centers, at which the RDT may be easily trapped [inset-1 of Fig. 6(a)], were observed during *in situ* TEM magnetizing experiments.

To study the MD configurations and their interaction with grain boundaries or defects, *in situ* experiments were carried out by tilting the specimens along different x/y directions to vary the in-plane field. The typical Foucault images obtained directly revealed the local remanence of specimen after magnetizing along the easy and heavy magnetic directions, as shown in Figs. 6(a) and 6(b), respectively. The in-plane magnetizing component of a magnetic field was proportional to the sinus of the tilt angle given in the images. Drastic changes in local remanence with respect to the direction of the applied field were clearly revealed, and can be qualitatively estimated from the ratio of the black to white regions of the Foucault images. Indeed, a well-developed domain structure with $D_u/D_d \approx 1$ is visible in Fig. 6(b), implying that the magnetic hysteresis effect in anisotropic Nd(Pr)–Fe–B magnets must be relatively small along the heavy magnetic axis. Corresponding differences in magnetic-microstructure features are apparent: the well-aligned region (area A in Fig. 6) remains well saturated, whereas the defect layer (area B) is far from such saturation. Since area B consists of nonaligned grains the associated domains may have different orientations in the absence of the magnetic field. A few very small reverse domains were found in area A, marked by arrow heads [also the inset of Fig. 6(a)]. Their presence is controlled by local imperfections, like inclusions or even misalignment of grains. In the latter case, the shape of the reverse domain is sensitive to such misalignment. It is clear from our *in situ* experiments that higher local remanence can be reached along the easy direction even with a smaller magnetic field applied to die-upset magnetic sample.

D. Determination of domain wall width

Many specific local features of MD configurations and DW motion depend on the thickness (δ_o) and interfacial energy (γ_w) of the 180°-Bloch DWs separating domains in hard anisotropic magnets. Thus, the determination of DW width is significant in understanding the magnetic properties of the materials. In the past, estimates of δ_o for the Nd–Fe–B phase were made by various indirect methods based on the equilibrium of minimum energy with respect to domain size, domain-wall energy, and saturation magnetization. More recently, an electron holographic technique was developed to directly measure the domain wall width by gauging the abrupt phase change across the domain wall.[17,18] However, electron holography, which involves phase reconstruction, is technically demanding and its application is limited to a very small area near a specimen edge. In contrast, the traditional Lorentz–Fresnel imaging method, which reveals domain-wall contrast, is easy to perform, although its usefulness has been overlooked recently. Therefore, we decided to reexamine the validity of Lorentz–Fresnel imaging in measuring the width of DWs. The DWs were imaged under ''out-of-focus'' conditions (objective lens off) with black- and white-line contrast (on a film positive), corresponding to

the so-called convergent (W_c) and divergent (W_d) walls, respectively. Simple analytical expressions for convergent and divergent-wall widths versus defocus value were given, for instance, in Ref. 19. The formula for divergent wall width is

$$W_d = \delta_o + 2z\Psi, \tag{2}$$

where z is the defocus value, and Ψ the deflecting angle caused by the action of Lorentz force on the electron beam. The value δ_o is determined straightforwardly as a linear asymptotic ($W_d \rightarrow \delta_o$) at zero defocus ($z \rightarrow 0$). Among three different approaches based on determining the width of a divergent-wall, a convergent-wall, or the difference in width of the two, we found that the determination of the divergent wall width is most reliable because it is valid for any $z>0$. Figure 7 gives an example of the experimental results. The numerical estimate gives $\delta_o = 5.8 \pm 2.8$ nm (best-fit parameters $P = 2{,}6 \times 10^{-4}$, N=6 and R=0.98 are the mean square deviation, number of experimental points and Student criteria), which agrees well with the theoretical estimate $\delta_o = \pi(A/K_1)^{1/2} = 4.2$ nm made using the exchange constant ($A = 7.7 \times 10^{-12}$ J/m) and the magneto-crystalline anisotropy constant ($K_1 = 4.3 \times 10^6$ J/m^3) for $Nd_2Fe_{14}B$ phase[20,21] at T=300 K.

E. HREM grain boundaries analysis

Our magnetic observations allow us to consider the interfaces between the c-axis aligned grains, i.e., pure [001] twist grain boundaries (twist GBs) as ''weak pinning centers'' for several reasons. First, HREM observations [Fig. 8(a)] revealed that twist GBs have a good lattice match of the basal plane of neighboring crystallites. In other words, there is very little or no intergranular phase at the twist GB; therefore, intergrain exchange coupling may occur. Second, the easy magnetic directions of such crystallites are parallel. This means that there is no need for activation energy related to moment rotation from one grain to another. As a result, big interacting magnetic domains, composed of many well-aligned grains with sizes below D_c, can be relatively easily formed in die-upset magnets (Fig. 2). Third, the DW usually run across such GBs close to a 90° configuration (Fig. 2). In this case, only a small part of DW at the point of intersection interacts with GBs. Hence, the increase of interaction energy again is minimal. In contrast to such observations, arbitrary grain boundaries with mixed tilt and twist characters in the nonaligned area (Fig. 5, area B) often exhibit intergranular crystalline phases [Fig. 8(b)], or amorphous phases [Fig. 8(c)]. Although we did not determine the composition and structure of the GB phase, which likely varies from boundary to boundary, for our current purpose of analyzing domain structure, we can assume that most of the not well-aligned NdFeB grains are surrounded by nonmagnetic intergranular phases that promote the exchange decoupling of grains. Such areas may act as potential pinning centers since, for RDT more energy will be needed to overcome a nonmagnetic thick intergranular layer and to rotate a magnetic moment in each grain from the local easy axis towards the common domain-magnetization direction. An example of such a pinned reverse domain is displayed in the inset of Fig. 6(a). The shape of the domain is determined by the local misalignment of grains, and by the well-visible 90°-DW/GB configurations mentioned above. An example of very strong pinning center expected for RDT motion across the GB, is shown in HREM image of Fig. 8(b). Apart of the presence of interfacial GB phase an additional 90° misorientation of easy magnetic axes in A and B crystallites [associated with local c axes in Fig. 8(b)] makes it extremely difficult for RDT to pass through such magnetic 90°-GB interface. It is expected to occur only by a single grain magnetic moment (m_s) rotation under the applied high field H_{int}. Theoretical estimate for such case[10,23] gives the value $H_{int} = 2K_1/I_s$ (where K_1 and I_s-anisotropy constant and saturation magnetization) numerically equal to anisotropy field $H_a = 73$ kOe for NdFeB phase.[7]

V. DISCUSSION

A. Grain alignment and remanence

The die-upset structure of Nd(Pr)–Fe–B magnets in general consists of platelet-shaped grains of the tetragonal 2-14-1 phase stacked in such a way that in general some preferential alignment with the c axis along the press (die upset) direction occurs.[1,2] This implies, in principle, both very strong texture and magnetic anisotropy of samples processed. The typical grain sizes, denoted as $\langle h \rangle$ for the averaged thickness along c axis, $\langle r \rangle$ for averaged width in the basal plane, and their aspect ratio $\langle h \rangle / \langle r \rangle$, may depend on the fabrication method and on the parameters used in the die-upset process, i.e., the magnitude of hot deformation displacement. In our case, $\langle h \rangle / \langle r \rangle \approx 1/4$–$1/6$. The averaged thickness of grains $\langle h \rangle \approx 100$–$150$ nm was less than the so-called single domain grain size $D_c = 1.4\ \gamma_w / M_s^2$ (where γ_w–DW energy and $4\pi M_s = 16.1$ kOe–saturated magnetization) estimated for $Nd_2Fe_{14}B$ magnets as 200[22] or 300 nm.[7] Under such conditions ($D < D_c$), extended interacting magnetic domains, running across several grains coupled with ferromagnetic exchange interactions, are observed (Fig. 2). Actually, this suggests a way to decrease total magnetic energy by ''switching off'' the increasing number of domain walls with specific energy (γ_w) when the dispersion in grain size becomes smaller than D_c. The pronounced texture of the main tetragonal 2-14-1 phase along the c axis (die-upset direction) serves as a common easy magnetization direction of the domain structure. This, in turn, allows increased remanence (I_r) of the anisotropic magnet much above the theoretical estimate $I_r = 1/2\ I_s$ made by Stoner–Wohlfarth[10] for isotropic hard magnets assuming a random distribution of noninteracting magnetic particles.

In order to get some estimate of remanence for anisotropic magnets in a first approximation we applied the following approach. We assumed by analogy to Ref. 10 that the remanence of anisotropic magnet is determined only by its crystallographic texture, i.e., the relative random misorientation of grains from the die-upset direction within some angle θ related to uniaxial texture ($0 < \theta < \theta_o$), and by neglecting the contribution due to exchange coupling of grains. Then, the relative remanence can be derived by the expression

$$I_r/I_s = m = 2\pi \int_0^{\theta o} \cos\theta \sin\theta \, d\theta \Big/ 2\pi \int_0^{\theta o} \sin\theta \, d\theta$$
$$= \frac{1}{2}(1+\cos\theta_o), \tag{3}$$

where θ_o is the maximal deviation angle of the texture and $n(\theta)d\theta = 2\pi \sin\theta d\theta$ is proportional to the number of atomic moments in the unit layer about the press direction with an angle between θ and $\theta + d\theta$. Here, we assume a random azimuthal distribution. It follows from this equation that for a random grain orientation the relative remanence $m=1/2$ ($\theta_o=90°$), and for a perfectly aligned grain structure $m=1$ ($\theta_o=0°$). Thus, in comparison with Ref. 10 the formula obtained is more general and takes into account the effect of grain texture or misorientation.

To characterize the contribution of defect layers (Figs. 4–6) to the magnetic structure of die-upset magnets, let us consider a special case when the grain structure has a periodical bimodal θ distribution: the A layers with well-aligned grains ($0<\theta_a \ll 90°$) of relative thickness $x_a=(1-x_b)$ along the press direction are separated by B layers of thickness (x_b) with pure grain alignment ($\theta_b \approx 90°$). Then, Eq. (3) can be modified to

$$I_r/I_s = m = \tfrac{1}{2}(1+\cos\theta_a)(1-x_b) + \tfrac{1}{2}(1+\cos\theta_b)x_b$$
$$\approx \tfrac{1}{2}(1+\cos\theta_a)(1-x_b) + \tfrac{1}{2}x_b. \tag{4}$$

Equations (3) and (4) may be of practical use for analysis of experimental data discussed below.

B. Reverse domains and domain walls

To better understand the experimental results we first discuss the concept of ''reverse domain tip'' (RDT). It is not very different from the well-accepted single DW concept, but may clarify some practical aspects of magnetization reversal.

In a general case, the domain walls in anisotropic magnets have a strong difference in speed of motion (displacement) along the easy and heavy magnetic directions. The reversals in magnetization is due to the motion of such domain walls or the expansion of reverse domains under the action of an external magnetic field. Each reverse domain, in turn, is surrounded by a couple of mirror-related domain walls, known as convergent (C) and divergent (D) ones in Lorentz microscopy. If magnetic spins inside these walls make some angle with the field direction, they, under the action of torque, start to rotate towards the field direction and effectively move away, leaving behind a space with reversed magnetization. Alternatively, the reverse magnetization can be imaged as the nucleation of the RDT, which generates a couple of split mirror related C/D walls, followed by the walls displacement in opposite directions. In this way RDT may play a key role since it can move very fast (without or with only very small activation energy) by pulling C/D walls across a uniform magnetic media along the easy magnetic direction unless pinned by structural defects, for instance, GBs in Figs. 3(c) or 6(a) and/or stopped by unfavorable magnetostatic stray fields [Fig. 2(b)]. Experimentally, it can be observed when the average domain size $D \gg \delta_o$.

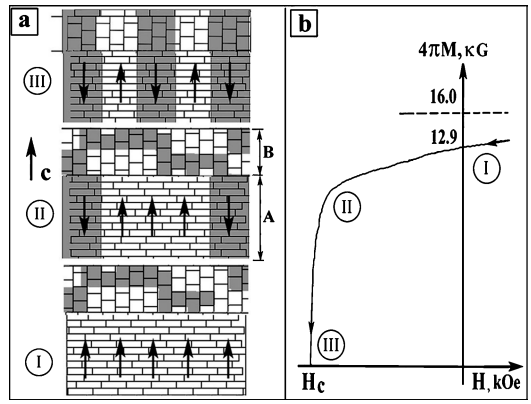

FIG. 9. Schematic drawing of the proposed defect-layered structure model (a) used to explain the role of defect layers in magnetization reversal of die-upset magnet (b). I, II, and III denote successive steps in magnetization reversal along a demagnetizing curve. The thick bricks represent the defect layer, while the thin bricks represent the well-aligned grain platelets.

According to estimate of DW width $\delta_o=5$ nm in $Nd_2Fe_{14}B$,[7] which is consistent with our experimental observations ($\delta_o=5.8\pm2.8$ nm, see Sec. IV D), the interfacial energy of DW in the 2-14-1 phase is high enough $\gamma_w=30$ mJ/m^2 ($\equiv 30$ erg/cm^2).[7] In general, the total magnetic energy of DW can be reduced by minimizing the number of local magnetic poles which increase magnetostatic energy. In other words, a DW should follow the local easy magnetic direction in microstructure as close as possible. In the case of well-aligned grains of 2-14-1 phase in die-upset magnets, it may be the common c-axis direction. Therefore, MD configurations have nearly always a strip-like shape in uniaxial magnetic materials, when viewed in cross-section sample with its major in-plane c-axis component of aligned grains perpendicular to the viewing direction. Each pass of a RDT through magnetic media will generate a new MD of opposite magnetization, i.e., a reverse domain. It is interesting to note that the width (or diameter) of nucleated RDT after splitting a couple of mirror-related DWs with thickness $\delta_o=5$ nm may be about $2\times2\delta_o=20$ nm. This estimate corresponds well to the critical diameter $D_o=2r_o=20$ nm of a spherical defect to nucleate a reverse domain proposed by Livingston[11] (for details, see Sec. II) to obtain a realistic estimate of $H_{ci} \sim 11$ kOe ($N_{eff}=1$) typical for sintered $Nd_2Fe_{14}B$ magnets. However, this approach may be more suited for interpreting the DW pinning mechanism in melt-spun ribbons since r_o may be interpreted as the characteristic grain size of $Nd_2Fe_{14}B$ for which surface tension impedes expansion of a reverse domain.

C. Microstructure-magnetic properties correlation

Strictly speaking, according to our observations, the so-called RDT may play a more important role in demagnetization processes than the simple DW motion itself for two reasons. (1) RDT is the most sensitive to field and is a flexible part of the MD configuration which can leave behind itself a couple of mirror related domain walls and may real-

ize a relatively easy magnetization reversal. (2) It is difficult to imagine a practical magnetization reversal by a simple pass of a single DW across the whole magnet since it contains plenty of defects acting as pinning centers for the domain wall motion. However, nucleation of reverse domains requires some higher activation energy and this process may be considered as a limiting stage in the high coercivity mechanism for delayed RDT nucleation and magnetization reversal. Intuitively, nucleation should occur near the imperfections which disturb the magnetic flux in the sample. The most suitable candidate for this type of imperfections are nonaligned or defect layers discussed above (Figs. 4 and 5). If we take into account that such layers may play a dual role—serving as nucleation centers of reverse domains, and also as pinning centers—it is clear why a single or even a few nucleated reverse domains cannot realize reversal of magnetization for the whole sample by the simple motion of generated DWs. All the RDTs and associated DWs will be impeded by the next nearest defect layer along the easy magnetic direction. Thus, the situation looks somewhat similar to the formation of periodical ''pinning potential'' due to presence of defect-layered superlattice along the easy axis. Here, the pinning potential implies a process of nucleation and pinning of reverse domains by the defect layers.

In order to verify the proposed mechanism of magnetization reversal, we made some estimates. According to the theory of magnetization, the domain reversal of single grain by rotation of magnetic moment will require a minimum field $H_{min}=K_1/I_s$[10,23] for the case of single grain tilted at 45° with respect to an applied magnetic field. For the $Nd_2Fe_{14}B$ phase, this amount is equivalent to an internal field 36.5 kOe. It follows from Fig. 4 that such grains with suitable 45° orientation may be easily found within defect layers containing a high fraction of nonmagnetic phases (inclusions, precipitates and even cavities). Strictly speaking, such defect layers should generate local demagnetizing fields due to the magnetostatic energy of free magnetic poles.[23] By assuming that the defect layers are similar to nonmagnetic cavities, a good approximation for the demagnetizing factor is $N_{eff}=1$.[23] Then, the external magnetic field $H_{ext}\approx H_c$ necessary to reverse the magnetization of 45°-tilted grains can be simply expressed as

$$H_c=H_{min}-N_{eff}I_s/\mu_o. \tag{5}$$

The numerical estimate from Eq. (5) in cgs units gives $H_c=(36.5-1\times16.1)$ kOe=20.4 kOe, which is close to the experimental value of $H_c=18.9$ kOe found for the sample under discussion (DU1418, MQ-3). Thus, we may assume that the high coercivity mechanism occurs via delayed nucleation of reverse domains near 45°-tilted grains, which belong to defect layers and exhibit a magnetization reversal by the rotation of local magnetic moment under applied reverse magnetic field. Further expansion of reverse domains along easy axis is limited by the nearest defect layer until the next delayed nucleation of reverse domains occurs (as schematically shown in Fig. 9), which in turn, may be governed by reverse domain expansion in well-aligned grain area by slow DWs motion along heavy axis or plane.

Our formula (5), derived on the basis of specific properties of defect layers, fits well to the coercivity formula suggested originally in Ref. 8 and modified recently by taking into account $H_N^{min}=K_1/I_s$[9] (see Sec. II for details). Hence, this can be considered as verifying such theoretical approach, and may allow a direct physical interpretation for some parameters used in this theory.

Now let us consider how the remanence $m=I_r/I_s$ of die-upset magnet may be related to the microstructural features. Our TEM observations revealed that the ratio of thickness of A to B layers in 50% die-upset sample (DU1418) was within B/A=(0.5–1.0) μm/(4.0–6.0) μm=0.083~0.25. In other words, the maximal relative thickness of the B-layer has to be about $x_b=0.25/(1+0.25)=0.2$. By substitution of $x_b=0.2$, Eq. (4) gives us

$$I_r/I_s=m=0.84=1/2[(1-x_b)(1+\cos\theta_a)+x_b], \tag{6}$$

from which an estimate of the expected texture angle for A layers gives $\theta_a=31.8°$. This value of texture angle is consistent with our TEM observations and fits well to the texture angle $\theta=32.3°$, determined as full-width at half-maximum (FWHM) of the rocking curve of (006) reflection and found recently for 50% die-upset Nd–Fe–B magnets by direct x-ray texture measurements.[24]

However, the reason, why a small density of reverse domains exists already at zero external fields, remains unclear. Perhaps the experimentally applied field was not strong enough to change their magnetization. Further in-depth investigations are needed to reveal the fine microstructure features of the permanent die-upset magnets and their relation to the structure-sensitive parameters analyzed in present work.

VI. CONCLUSION

Magnetic-sensitive Foucault images obtained during *in situ* TEM observations of die-upset hard magnets $Nd_{13.75}Fe_{80.25}B_6$ and $Pr_{13.75}Fe_{80.25}B_6$ characterized by high energy product indicate the presence of quasi-periodic nonaligned ''extended defect layers'' transverse to press direction. The local remanence of such defect layers is far away from saturation at zero magnetic field. The layers are enriched with inclusions of approximate composition Nd_7Fe_3, and are associated with original ribbon interfaces present in the bulk of hard magnets. The experimental data allowed us to conclude that such extended defect layers may play an important role in the high coercivity mechanism caused by delayed nucleation of reversed domains in die-upset magnets.

ACKNOWLEDGMENTS

This research was supported by the U.S. Department of Energy, Division of Materials, Office of Basic Energy Science, under the Contract No. DE-AC02-76CH0016.

[1] R. K. Mishra, E. G. Brewer, and R. W. Lee, J. Appl. Phys. **63**, 3528 (1988).
[2] R. K. Mishra, J. Appl. Phys. **62**, 967 (1987); R. K. Mishra, Mater. Sci. Eng., B **7**, 297 (1991).
[3] M. Sagawa and S. Hirosawa, Mater. Res. Soc. Symp. Proc. **96**, 161

(1987); M. Sagawa, S. Fujimura, N. Togawa, H. Yamamoto, and Y. Matsuura, J. Appl. Phys. **55**, 2083 (1984).
[4] R. Ramesh, G. Thomas, and B. M. Ma, Acta Metall. **37**, 1421 (1989).
[5] A. Yan, X. Song, Z. Chen, and X. Wang, J. Magn. Magn. Mater. **185**, 369 (1998).
[6] S. Hirosawa, K. Tokuhara, Y. Matsuura, H. Yamamoto, S. Fujimura, and M. Sagawa, J. Magn. Magn. Mater. **61**, 363 (1986).
[7] J. F. Herbst, Rev. Mod. Phys. **63**, 819 (1991).
[8] K.-D. Durst and H. Kronmuller, J. Magn. Magn. Mater. **59**, 86 (1986); H. Kronmuller, K.-D. Durst, and M. Sagawa, J. Magn. Magn. Mater. **74**, 291 (1988).
[9] A. Zern, M. Seeger, J. Bauer, and H. Kronmuller, J. Magn. Magn. Mater. **184**, 89 (1998).
[10] E. C. Stoner and E. P. Wohlfarth, Philos. Trans. R. Soc. London, Ser. A **240**, 599 (1948).
[11] J. D. Livingston, in *Proceedings of the Eighth International Workshop on Rare-Earth Magnets and Their Applications*, edited by K. J. Strnat (University of Dayton, Dayton, Ohio, 1985), p. 423.
[12] V. Villas-Boas, J. M. Gonzalez, F. Cebollada, M. F. Rossignol, D. W. Taylor, and D. Givord, J. Magn. Magn. Mater. **185**, 180 (1998).
[13] D. Givord, P. Tenaud, and T. Vaidieu, IEEE Trans. Magn. **MAG-24**, 1921 (1988).
[14] ''Magnequench'' Catalogue, Oct. 1994, printed in U.S.A.; see also L. H. Lewis, J. Gao, D. C. Jiles, and D. O. Welch, J. Appl. Phys. **79**, 6470 (1996).
[15] R. W. Lee, Appl. Phys. Lett. **46**, 790 (1985).
[16] R. W. Lee, E. G. Brewer, and N. A. Schaffel, IEEE Trans. Magn. **MAG-21**, 1958 (1985); C. D. Fuerst and E. G. Brewer, J. Appl. Phys. **73**, 5751 (1993).
[17] M. R. McCartney and Y. Zhu, Appl. Phys. Lett. **72**, 1380 (1998).
[18] Y. Zhu and M. R. McCartney, J. Appl. Phys. **84**, 3267 (1998).
[19] R. H. Wade, Proc. Phys. Soc. **79**, 1237 (1962).
[20] T. Schrefl and J. Fidler, J. Appl. Phys. **79**, 6458 (1996).
[21] M. K. Griffiths, J. E. L. Bishop, J. W. Tucker, and H. A. Davies, J. Magn. Magn. Mater. **183**, 49 (1998).
[22] D. D. Mishin, *Magnetic Materials* (in Russ.) (High School, Moscow, 1991), p. 284.
[23] S. Chikazumi, *Physics of Magnetism* (R. E. Krieger, Malabar, FL), p. 554.
[24] Y. R. Wang, S. Guruswamy, and V. Panchanathan, J. Appl. Phys. **81**, 4450 (1997).